ISSN 1392-1320 MATERIALS SCIENCE (MEDŽIAGOTYRA). Vol. XX, No. X. 2027

A Study on the Acoustic Properties of Glass Fiber-Melamine Foam Composites Based on TMM and FE-SEA

Weizheng LIU, Jintao SU *

College of Automotive and Electrical Engineering, Harbin Cambridge University, 239 Haping Road, Xiangfang District, Harbin 150000, China

http://doi.org/10.5755/j02.ms.44783

Received 23 April 2026; accepted 15 August 2026

To address the challenge of broadband noise control in electric vehicle doors under the constraints of narrow installation space and lightweight design, this study focuses on unreinforced glass fiber-melamine foam (GF-MF) composites and systematically investigates their acoustic performance regulation mechanisms and engineering structural design for vehicle door applications. Combining the Transfer Matrix Method (TMM) with impedance tube experiments, the effects of porosity, air backing layer thickness, and flow resistivity on the acoustic coefficients of the material were analyzed. A hybrid Finite Element-Statistical Energy Analysis (FE-SEA) model was established to evaluate the sound transmission loss (STL) of five door composite layup schemes under diffuse incidence conditions. The results demonstrate that high porosity significantly optimizes the impedance matching characteristics in the mid-to-high frequency range and enhances broadband sound absorption efficiency, while high flow resistivity effectively strengthens the viscous dissipation capacity in the mid-to-low frequency range. Among all structural layup schemes, the pure air layer scheme yields the highest STL across the full frequency band. Adding a 2 mm viscoelastic damping layer on the outer door panel side further improves low-frequency sound insulation performance. In contrast, positioning the damping layer adjacent to the GF-MF side or adopting a honeycomb sandwich structure leads to acoustic performance degradation. This research elucidates the acoustic parameter regulation laws of glass fiber-melamine foam (GF-MF) composites and the optimization strategies for vehicle door layup designs. A systematic comparative analysis of five layup schemes under identical thickness constraints is conducted. The findings provide practical engineering guidance for the development of lightweight, thickness-constrained acoustic packages in electric vehicle door systems.

Keywords: composite materials, transfer matrix method, statistical energy analysis, vehicle door acoustic package.

1. INTRODUCTION

As the global automotive sector rapidly advances toward electrification, battery electric vehicles have dispensed with conventional internal combustion engines, consequently forfeiting the inherent masking effect that engine noise traditionally offers against road and aerodynamic noise. This shift makes external noise permeation through the vehicle body more noticeable. As a result, NVH (Noise, Vibration, and Harshness) management has become a critical determinant of a vehicle's competitive standing. In electric vehicles, the predominant contributors to interior noise are tire-road interaction (road noise) and aerodynamic airflow (wind noise), with frequency components spanning approximately 200 to 3000 Hz. The interior sound pressure levels typically range from 60 to 85 dB. In automotive engineering, door panels are typically required to achieve a sound transmission loss of at least 25 dB in the 100 – 1000 Hz range to ensure occupant comfort. As the most substantial access point within the vehicle body, car doors constitute the principal conduit through which road and wind noise infiltrate the passenger compartment. The acoustic packages integrated within these doors, characterized by their sound absorption and insulation properties, play a critical role in determining the overall comfort of the cabin environment. Nonetheless, the industry faces pervasive challenges. These include limited broadband noise attenuation in constrained spatial configurations and the complex trade-off between weight reduction and acoustic efficacy. Therefore, the advancement of noise mitigation materials and the development of novel structural designs have emerged as pressing research priorities within the automotive sector.

International research on the simulation of acoustic properties in multilayer composite materials and their applications in the automotive industry commenced at an earlier stage, resulting in a comparatively well-established research framework. This foundation has facilitated the development of a comprehensive and mature set of theories and methodologies. Andrea S. et al. [1] introduced a hybrid analytical approach grounded in the Johnson-Champoux-Allard-Lafarge (JCAL) model to evaluate recycled fiber composites employed in automotive contexts. Through the determination of effective density and fiber radius, they were able to forecast the acoustic characteristics of these materials. The validity and robustness of this methodology were substantiated by a series of experimental investigations. Jiang Y. et al. [2] employed the NOVA module within the VA ONE software to examine the acoustic characteristics of layered materials with different thicknesses. Their study combined theoretical simulations with experimental validation, thereby demonstrating the module's capability to accurately predict the acoustic behavior of multilayer composite materials. Kim J. et al. [3] developed a lightweight superpanel featuring a multi-scale lattice sandwich architecture that exhibits broadband sound

* Corresponding author: J. Su
E-mail: *11947@hbuas.edu.cn*

absorption by leveraging negative effective material properties. This design achieves a sound transmission loss greater than 16.7 dB within the frequency range of 100 to 1,750 Hz, while maintaining a mass per unit area that is merely one-twentieth that of a steel panel, demonstrating comparable noise reduction capabilities. Sangiuliano L. et al. [4] utilized metal additive manufacturing to fabricate resonant metamaterials aimed at mitigating noise associated with the 230 Hz acoustic resonance of tires. This approach effectively attenuates tire-generated noise within the vehicle cabin while providing a lightweight substitute for conventional damping systems. Jung J. et al. [5] developed an attachable local resonator (ALR) and designed its acoustic-vibration bandpass filter utilizing finite element unit cell analysis. The effectiveness of the ALR in reducing vibration and noise was subsequently validated through in-vehicle testing on an automotive dashboard. Kronowetter F. et al. [6] have engineered an innovative composite material and metamaterial wheel liner aimed at mitigating tire noise. By employing an integrated design approach that combines porous layers with micro-perforated plates, they substantially enhanced acoustic attenuation within the 800 – 4000 Hz frequency spectrum. This design not only effectively expanded the bandwidth of low-frequency sound absorption but also achieved superior noise reduction at targeted frequencies. O'Boy M. [7] introduced an expedited design approach grounded in the one-dimensional waveguide equation to optimize the parameters of a wheel-mounted Helmholtz resonator. Utilizing three arrays of tuned resonators, the researchers achieved a reduction in the peak sound pressure level from 103 dB to 88 dB over a vehicle speed interval of 54 to 108 km/h. Hwang, H. et al. [8] introduced a statistical modal energy analysis approach that extends the application of statistical energy analysis to the mid-frequency domain. They formulated power balance equations between the modes of distinct subsystems, enabling an effective characterization of the impact of dissipative materials on acoustic-vibrational behavior in the mid-frequency range.

Despite the relatively recent inception of domestic research in this domain, it has progressed swiftly and attained substantial achievements in both theoretical advancements and practical engineering applications. Su, J. et al. [9] conducted an investigation into the multi-layer composite configurations of automotive firewalls, formulating propagation equations for plane waves within both single-layer and double-layer media. Utilizing numerical simulations alongside impedance tube experiments, they elucidated the influence of air layer thickness on sound transmission loss across diverse multi-layer structural arrangements. Zhou G. et al. [10] have developed a structural design for a multi-mode anti-resonant cooperative thin-film acoustic metamaterial aimed at mitigating low-frequency noise within vehicles. This design demonstrates the capability to achieve an average noise attenuation of 3 dB(A) for engine noise frequencies below 1 kHz. Wang, X. et al. [11] developed a multi-layered sound-absorbing composite material incorporating a variable cross-section cavity. Optimization experiments utilizing algorithmic approaches demonstrated that the Improved Particle Swarm Optimization algorithm exhibits superior performance compared to the Artificial Fish Swarm Algorithm in enhancing the material's low-frequency sound absorption characteristics. Shen L. et al. [12] employed an environmentally sustainable method to integrate cellulose nanofibers with melamine foam. By optimizing sound energy dissipation via a hierarchical pore architecture, they achieved an enhancement in the material's sound absorption capacity by approximately 107 % at 500 Hz, alongside an 80 % increase in the noise reduction coefficient. Aiming at the design requirements of thin acoustic absorbers, Shen, X. et al. [13] developed an optimized multilayer compressed porous metal absorber with a rear cavity, whose total thickness is only 5 mm. Based on the Johnson-Champoux-Allard model and the cuckoo search algorithm, the proposed absorber achieves an average sound absorption coefficient of 0.5105 in the frequency range of 100 to 6000 Hz. Wan Q. et al. [14] performed both simulation and experimental investigations on an integrated automotive thermoelectric generator, revealing that the system effectively integrates superior high-frequency noise attenuation capabilities alongside a power output of 515 W. Shen J. et al. [15] developed a multi-layer stacked acoustic device without packaging, resulting in an ultra-compact filter centered at 2.14 GHz. This work highlights the effectiveness of multi-layer structural designs in advancing the miniaturization of acoustic devices. Otaru A J. et al. [16] proposed a predictive model for the sound absorption characteristics of honeycomb sound-insulating materials utilizing a backpropagation artificial neural network. The model demonstrated a correlation exceeding 95 % with empirical measurements, thereby offering a robust and efficient analytical approach for the industrial design of sound-insulating materials.

In summary, although considerable progress has been made worldwide in acoustic modeling, structural design, and algorithmic simulation of multilayer composite materials, prominent research gaps still exist. Studies abroad are mostly tailored to European and American vehicle models. Domestic research tends to focus on single-parameter or single-performance analyses. However, most of the above-mentioned studies have limitations: they do not systematically investigate the sound insulation performance of multilayer composites within the confined space of vehicle doors (total thickness $\leq$ 45 mm), nor do they provide direct comparisons of different layup schemes (e.g., air layer, honeycomb layer, damping layer position) under identical constraints. Neither has sufficiently investigated the full-frequency acoustic regulation mechanisms of composite materials within the confined narrow space of vehicle doors, nor has it developed specialized design solutions suitable for such constrained space. Accordingly, this paper aims to address the pain points in the acoustic package design of electric vehicle doors, and conducts research from three core aspects: material parameter optimization, acoustic performance analysis, and laminate structure evaluation.

2. THEORETICAL METHODS IN ACOUSTICS

2.1. Fundamental principles of plane wave propagation

A plane wave is the simplest mode of sound propagation in a homogeneous medium. Under the small-amplitude linear acoustics approximation, the medium is assumed to be ideal (inviscid, homogeneous, isotropic) and the sound propagation adiabatic. The one-dimensional plane wave equation can be systematically derived [17]:

$$\frac{\partial^2 p}{\partial x^2} = \frac{1}{c_0^2}\frac{\partial^2 p}{\partial t^2}, \tag{1}$$

where p is the instantaneous sound pressure within the medium, measured in pascals (Pa); x is the spatial coordinate along the direction of sound propagation; t corresponds to the propagation time; c_0 is the speed of sound in air (343 m/s). For a steady-state harmonic sound field, the solution of the wave equation can be written as:

$$p(x,t) = \hat{p}(x) \cdot e^{j\omega t}. \tag{2}$$

Substituting Eq. 2 into Eq. 1 yields the Helmholtz equation:

$$\frac{d^2\hat{p}(x)}{dx^2} + k_0^2\hat{p}(x) = 0; \tag{3}$$

where $k_0 = \frac{\omega}{c_0}$ is the wave number. The general solution is:

$$\hat{p}(x) = P_i e^{-jk_0 x} + P_r e^{jk_0 x}, \tag{4}$$

where P_i and P_r are the complex amplitudes of incident and reflected waves.

$$p(x,t) = P_i e^{j(\omega t - k_0 x)} + P_r e^{j(\omega t + k_0 x)}. \tag{5}$$

Using the linearized Euler equations, the particle velocity is:

$$v(x,t) = U_i e^{j(\omega t - k_0 x)} - U_r e^{j(\omega t + k_0 x)}. \tag{6}$$

The acoustic impedance is defined as the ratio of sound pressure to particle velocity at a given location:

$$Z_s = \frac{p(x,t)}{v(x,t)}. \tag{7}$$

2.2. Theory of transfer matrix method

The Transfer Matrix Method (TMM) is a fundamental approach for multilayered media. Considering an incident wave x impinging upon the material at a specified angle θ_0 of incidence, the theoretical representation of the composite material is illustrated in Fig. 1.

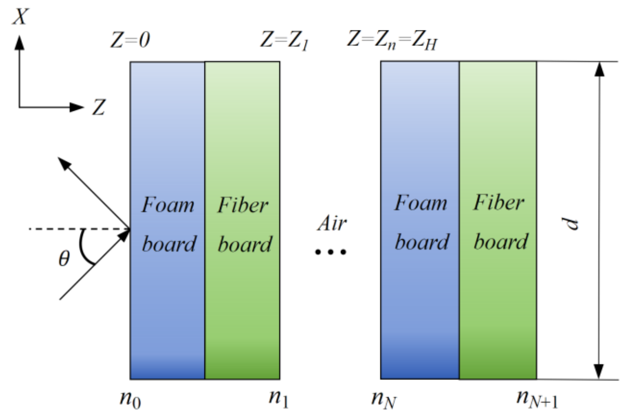

Fig. 1. Schematic diagram of multilayer composite material

It is also assumed that the composite interface is a plane parallel to each other, the interface is marked as $z = z_n$, and the outermost layer of the structure is a semi-infinite uniform medium. A plane wave (frequency is f) is incident at an incident angle θ_0, defined in the x-o-z coordinate system. Meanwhile, the sound pressure in each layer of the composite material is p_n, and the sound velocity of normal direction is v_{nz}, wherein the subscript n represents the number of composite material layer. The sound pressure p_n can be expressed as [18]:

$$p_n = a_n e^{ik_n x \sin\theta_n + ik_n z \cos\theta_n} + b_n e^{ik_n x \sin\theta_n - ik_n z \cos\theta_n} \tag{8}$$

The limited condition is that the sound pressure and the sound velocity of normal direction are continuous at the interface:

$$p_n = p_{n+1}, v_{nz} = v_{(n+1)z}(z = z_n). \tag{9}$$

The transfer matrix is a relationship matrix between p_n and v_{nz} in two adjacent interfaces, and in the subsequent derivation process, the factor $e^{ik_n x \sin\theta_n}$ is omitted because the operation of the x coordinate is not involved, then the following matrix is obtained:

$$q_n = \begin{pmatrix} p_n \\ v_{nz} \end{pmatrix} = \begin{pmatrix} a_n e^{ik_n z \cos\theta_n} + b_n e^{-ik_n z \cos\theta_n} \\ \frac{1}{z_n}\left(a_n e^{ik_n z \cos\theta_n} - b_n e^{-ik_n \cos\theta_n}\right) \end{pmatrix}, z_n = \frac{d_n c_n}{\cos\theta_n} = \frac{E_n}{\cos\theta_n}, \tag{10}$$

where Z_n is the acoustic impedance of normal direction; d_n is the density of the n-th layer composite; E_n is the elastic modulus of the n-th layer composite. The matrixes of the upper and lower surfaces of the n-th composite material are respectively denoted as q_n^{up} and q_n^{down}, and the Eq. 10 is applied to the interface of the incident layer ($z = 0$) and the interface of the transmission layer ($z = H$):

$$q_0^{up} = \begin{pmatrix} 1 + R_p \\ \frac{1}{z_0}(1 + R_p) \end{pmatrix}, q_{(N+1)}^{down} = \begin{pmatrix} T_p \\ \frac{T_p}{z_{N+1}} \end{pmatrix}, \text{ and } q_{(N+1)}^{down} = T \cdot q_0^{up}, \tag{11}$$

where T is the transfer matrix between q_n^{up} and q_n^{down}, which is a second-order square matrix. It is proved below that T is the transfer matrix between the incident surface and the exit surface of the composite. The sound pressure reflection coefficient can be obtained as follows:

$$R_p = \frac{\left(T_{11} + \frac{1}{z_0}T_{12}\right) - z_{N+1}\left(T_{21} + \frac{1}{z_0}T_{22}\right)}{z_{N+1}\left[\left(T_{21} - \frac{1}{z_0}T_{22}\right) - \frac{1}{z_{N+1}}\left(T_{11} - \frac{1}{z_0}T_{12}\right)\right]}. \tag{12}$$

Then the acoustic energy reflection coefficient R_e and sound absorption coefficient α can be obtained as follows:

$$R_e = \left|R_p\right|^2 \cdot \frac{z_0}{z_{N+1}}, \alpha = 1 - R_e \cdot R_e^*. \tag{13}$$

According to Eq. 10, the matrix of the n-th layer can be expressed as:

$$q_n^{down} = \begin{pmatrix} e^{ik_n z\cos\theta_n} & e^{-ik_n z\cos\theta_n} \\ \frac{e^{ik_n z\cos\theta_n}}{z_n} & \frac{-e^{-ik_n z\cos\theta_n}}{z_n} \end{pmatrix}_{z=z_{n-1}} \begin{pmatrix} a_n \\ b_n \end{pmatrix}, q_n^{up} = \begin{pmatrix} e^{ik_n z\cos\theta_n} & e^{-ik_n z\cos\theta_n} \\ \frac{e^{ik_n z\cos\theta_n}}{z_n} & \frac{-e^{-ik_n z\cos\theta_n}}{z_n} \end{pmatrix}_{z=z_n} \begin{pmatrix} a_n \\ b_n \end{pmatrix}. \quad (14)$$

According to boundary conditions of the composite sound absorbing system, the matrixes q_n above the n-th layer material and under the $(n+1)$-th layer material have the following relationship: $q_n^{up}=q_{n+1}^{down}=E_n$, it can be obtained: $E_n=t_n \cdot E_{n+1}$. T_n is the transfer matrix of the n-th layer material, and the specific form is:

$$t_n \begin{pmatrix} \cos O_n & iz_n \sin O_n \\ \frac{i}{z_n}\sin O_n & \cos O_n \end{pmatrix}, \quad (15)$$

where $O_n=k_n \mathrm{h}_n cos\theta_n$. From Eq. 10 to Eq. 15, the relationship between the total transfer matrix T and the transfer matrix t_n of each layer is obtained:

$$T = t_n \cdot t_{n+1} \cdot \ldots \cdot t_2 \cdot t_1 . \quad (16)$$

2.3. Fundamental principles of statistical energy analysis

Statistical Energy Analysis (SEA) predicts vibration transmission and energy dissipation in structure-acoustic coupled systems, especially effective for high-frequency analysis of complex structures. For a subsystem, the dissipated power is [19]:

$$P_{\mathrm{d\,iss}} = \omega \eta E , \quad (17)$$

where ω is the central frequency of the frequency band; h is the average loss factor associated with that frequency band; E corresponds to the energy of the vibrating system.

In engineering practice, a system is usually divided into multiple subsystems that exchange energy. Fig. 2 illustrates the energy coupling relationships in a twin-system SEA model.

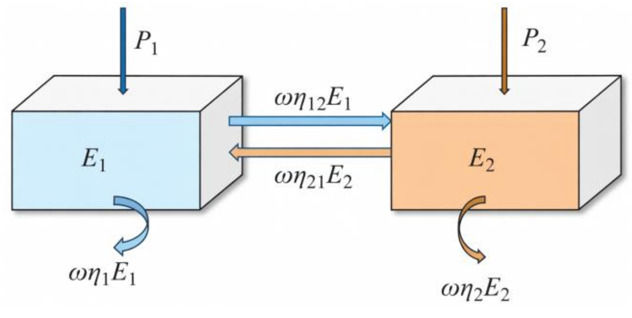

Fig. 2. Illustrative diagram depicting energy coupling within the twin-system model of SEA

The power balance equations for two coupled subsystems are:

$$\begin{cases} P_1 = \omega\eta_1 E_1 + \omega\eta_{12} E_1 - \omega\eta_{21} E_{21} \\ P_2 = \omega\eta_2 E_2 + \omega\eta_{21} E_2 - \omega\eta_{12} E_1 \end{cases} ; \quad (18)$$

$$\omega \begin{bmatrix} \eta_1 + \eta_{12} & -\eta_{12} \\ -\eta_{21} & \eta_2 + \eta_{21} \end{bmatrix} \begin{bmatrix} E_1 \\ E_2 \end{bmatrix} = \begin{bmatrix} P_1 \\ P_2 \end{bmatrix} , \quad (19)$$

where P_1 and P_2 are the input power supplied by the external excitation source to subsystem 1 and subsystem 2, respectively; E_1 and E_2 correspond to the energy stored within subsystem 1 and subsystem 2, respectively; η_1 and η_2 signify the internal loss factors associated with subsystem 1 and subsystem 2, respectively; η_{12} and η_{21} represent the coupling loss factors characterizing the energy exchange between subsystem 1 and subsystem 2.

Using the internal loss factor, coupling loss factor, and input power, the average energy level of the subsystem is obtained, from which the sound insulation performance is assessed. The sound power radiated into half-space is then determined by solving the power-frequency-flux balance equations.

2.4. Theory of the hybrid SEA-FE algorithm

SEA requires high modal density, which may not hold in the low-to-mid frequency range. The hybrid FE-SEA method combines finite element analysis for deterministic subsystems with SEA for statistical subsystems.

According to the principle of energy conservation, the power balance equation for the coupled FE-SEA system can be expressed as follows [19]:

$$P_{\mathrm{in,\,d\,ir}}^{(m)} = P_{out,\;rev}^{(m)\mathrm{d\,iss,\,m}} , \quad (20)$$

where $P_{\mathrm{in,\,d\,ir}}^{(m)}$ is the input power within the direct field; $P_{\mathrm{out,\,rev}}^{(m)}$ is the power dissipated by the direct field as it executes work at the boundary constraints; $P_{\mathrm{d\,iss,\,m}}$ corresponds to the energy loss occurring within the subsystem.

$$\left\langle S_{qq} \right\rangle = D_{\mathrm{d\,ir}}^{-1} \left(S_{ff}^{\mathrm{ext}} + \sum \frac{4E_m}{\pi\omega n_m} \mathrm{Im}\left\{ D_{\mathrm{d\,ir}}^{(m)} \right\} \right) D_{\mathrm{d\,ir}}^{-\mathrm{H}} . \quad (21)$$

This results in the dynamic displacement response $\langle S_{qq} \rangle$ at each node within the finite element (FE) subsystem. In the corresponding equation, $D_{\mathrm{d\,ir}}$ represents the joint overall stiffness matrix encompassing the direct field interactions between the Statistical Energy Analysis (SEA) subsystem and the FE subsystem; S_{ff}^{ext} denotes the external force applied to the FE subsystem; E_m corresponds to the energy of the m-th SEA subsystem; H designates the conjugate transpose of the matrix. From these parameters, key system characteristics such as transmission loss and radiated sound power can be derived.

3. ACOUSTIC STRUCTURAL DESIGN AND PERFORMANCE TESTING METHODS

The door acoustic system of an all-electric vehicle serves as the principal conduit for the transmission of external road and wind noise into the cabin. Consequently, it is imperative that this system delivers broadband noise attenuation across the frequency spectrum of 10 to 5,000 Hz. This performance must be achieved within a constrained installation depth ranging from 20 to 45 mm, while simultaneously satisfying the stringent environmental durability standards characteristic of the automotive industry. The sound absorption properties of porous materials are predominantly described by the normal sound absorption coefficient and the characteristic acoustic impedance. These parameters are collectively influenced by the inherent properties of the material as well as the external environmental conditions. Acoustic testing is classified into three distinct scenarios based on variations in sound wave incidence conditions: normal incidence, oblique incidence, and diffuse incidence. The impedance tube method is capable of precisely measuring the acoustic properties of materials under normal incidence conditions. This technique provides a controlled testing environment and ensures high reproducibility, thereby establishing itself as the predominant approach for characterizing intrinsic material properties at the laboratory scale. Conversely, the reverberation chamber method effectively simulates diffuse sound fields typical of real-world engineering contexts, making it well-suited for comprehensive evaluation of engineered sound absorption and sound insulation performance. Together, these two methodologies offer complementary strengths, furnishing robust support for the accurate design and performance optimization of acoustic packaging materials used in vehicle doors.

The effectiveness of sound insulation is influenced by both the reflection of sound waves and the internal absorption properties of the material, with key determinants being the material's areal density and acoustic impedance characteristics. Materials possessing high areal density generally demonstrate superior sound reflection abilities, whereas porous materials that exhibit favorable impedance matching with air can effectively dissipate sound energy via viscous friction and thermoelastic mechanisms. Fig. 3 depicts the installation sites and composite arrangement of the two materials on the inner door panel, elucidating their spatial configuration as the sound-receiving impedance-matching layer and the primary dissipation layer.

Fig. 3. Schematic diagram of the impedance tube experiment principle [20]

In response to the dual objectives of reducing weight and achieving broadband noise attenuation in electric vehicle door applications, the present study examines an unreinforced fiberglass-melamine foam multilayer composite as the core substrate. This investigation aims to explore acoustic structural design strategies and methods for performance characterization.

3.1. Selection of acoustic materials and structural design

3.1.1. Selection of substrates and characterization of basic performance parameters

In accordance with the design requirements for acoustic packages in pure electric vehicle doors, unreinforced glass fiber (GF) and melamine foam (MF) were selected as the core materials for the composite structure. Both materials possess established commercial viability within the automotive acoustics industry and exhibit complementary acoustic properties, rendering them well-suited to address the broadband noise reduction demands of vehicle doors. GF functions as the primary sound-absorbing and dissipative layer, characterized by an internally interconnected three-dimensional random fiber pore network that facilitates efficient viscous friction and thermoelastic dissipation of mid-to-high-frequency sound waves. Due to its elevated porosity and viscoelastic damping characteristics, MF functions effectively as an impedance-matching layer on the sound-receiving surface, thereby minimizing interface reflections and dissipating low-frequency acoustic energy via structural resonance. The fundamental physical and acoustic properties of these two base materials are summarized in Table 1.

Table 1. Input parameters for material simulations

Material parameter	Unreinforced fiberglass-5.5 kg/m^3	Melamine foam-8.8 kg/m^3
Porosity	0.94	0.99
Flow resistivity	20000	10900
Tortuosity	1.2	1.02
Viscous characteristic length, m	5.2×10^{-5}	1.0×10^{-4}
Thermal characteristic length, m	1.04×10^{-4}	1.3×10^{-4}
Solid density, kg/m^3	5.5	8.8
Poisson ratio	0	0.4

3.1.2. Design of composite structure layup schemes

Drawing upon the principles of impedance gradient matching and the synergistic effects of vibration damping in porous media acoustics, this study proposes a multi-layer composite structure composed of a "sound-receiving matching layer-core dissipation layer-core/damping tuning layer." In this configuration, MF functions as the impedance matching layer on the sound-receiving surface, GF serves as the core dissipation layer, and the honeycomb core layer (24 kg/m^3) provides a lightweight yet high-stiffness framework to mitigate low-frequency structural sound transmission. Additionally, a viscoelastic polymer damping layer is incorporated to further attenuate vibrations of the steel plate. Concurrently, the Helmholtz resonance phenomenon within the air layer is exploited to optimize low-frequency sound absorption, while the steel plate contributes essential structural stiffness and mass for low-frequency sound insulation. This design departs from the conventional binary model of "sound-absorbing layer + sound-insulating layer" by introducing a multi-component synergistic mechanism that integrates core, damping, sound absorption, and sound insulation functionalities. The overall thickness of all configurations is rigorously maintained within 45 mm. The steel door plate thickness is fixed at 1 mm, and the combined thickness of the GF-MF composite remains constant at 25 mm; the sole variable is the 19 mm intermediate layer situated between the inner and outer panels. Adhering to the single-variable principle, five comparative configurations were developed, as detailed in Table **2**.

Table 2. Design of a multi-layer composite structure for vehicle doors

Scheme number	Structure layers (from the exterior to the interior)	Key variables
1	1 m steel + 19 mm air + 10 mm GF +15 mm MF	–
2	1 mm steel + 19 mm aluminum-honeycomb + 10 mm GF +15 mm MF	Honeycomb material
3	1 mm steel + 19 mm honeycomb + 10 mm GF +15 mm MF	Honeycomb material
4	1 mm steel + 2 mm visco-elastic polymer+ 17 mm air + 10 mm GF +15 mm MF	Location of the damping layer
5	1 mm steel + 17 mm air + 2 mm visco-elastic polymer + 10 mm GF +15 mm MF	Location of the damping layer

Scheme 1 functions as the baseline control group to assess the enhancement in sound insulation provided by the alternative configurations. Scheme 2 and 3 employ aluminum honeycomb panels and conventional honeycomb panels, respectively, to compare the acoustic performance associated with different honeycomb core materials, leveraging their lightweight and high-stiffness characteristics to mitigate low-frequency structure-borne noise. Schemes 4 and 5 maintain a consistent total thickness of 19 mm for the combined air and damping layers, while varying the positioning of the viscoelastic polymer (butyl rubber)-with Scheme 4 placing it adjacent to the outer door panel and Scheme 5 positioning it adjacent to the GF-MF side-in order to examine the influence of damping layer placement on the attenuation of low-frequency structural sound transmission.

3.2. Acoustic performance testing and simulation modeling

3.2.1. Testing of sound absorption performance using the impedance tube method

The impedance tube method represents a highly accurate experimental approach for measuring the normal incidence sound absorption coefficient and characteristic acoustic impedance of materials, in strict compliance with the ISO 10534-2 standard. The frequency range employed in the tests spans from 10 to 5000 Hz, thereby encompassing the principal noise frequency spectrum (50 – 4000 Hz) relevant to interior door panels of new energy vehicles. The experimental apparatus comprises an impedance tube, a loudspeaker, a power amplifier, two microphones, a data acquisition system, and specialized acoustic analysis software. The loudspeaker generates a steady-state harmonic plane wave, while the power amplifier serves to enhance the amplitude of the excitation signal. The pair of microphones are positioned at predetermined locations within the impedance tube to simultaneously record sound pressure signals. Subsequently, the data acquisition system converts these acoustic signals into electrical signals, which are then processed by the analysis software to yield the desired acoustic parameters. Illustrative schematics of the overall experimental setup and its principal components are provided in Fig. 4 and Fig. 5.

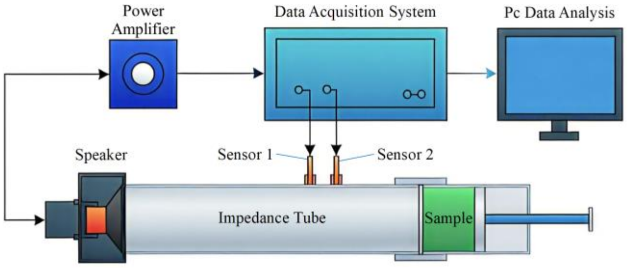

Fig. 4. Schematic diagram of the impedance tube experiment principle

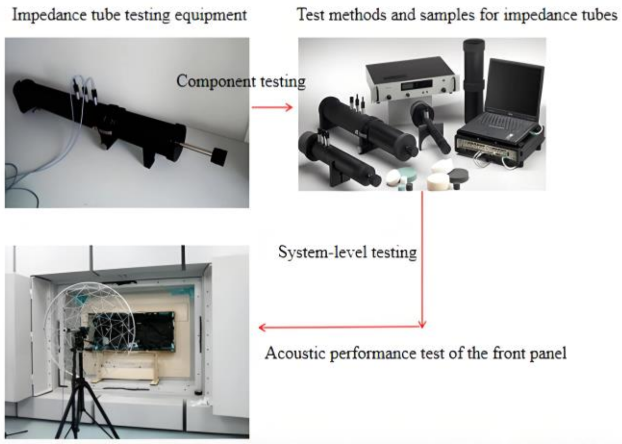

Fig. 5. Component testing and system testing methods for acoustic package materials [21]

The testing procedure is grounded in the theoretical framework of one-dimensional plane wave propagation and aligns with the fundamental principles of the transfer matrix method. A plane wave, generated by loudspeaker excitation, impinges upon the specimen surface along the longitudinal axis of the impedance tube. Within the material, a portion of the acoustic energy is attenuated due to viscous friction and thermoelastic relaxation phenomena, whereas the remaining acoustic energy is reflected specularly by the rigid backing located at the rear of the specimen. The resultant sound field inside the impedance tube arises from the superposition of the incident and reflected waves. By employing dual microphones to measure the spatial distribution of sound pressure, it is possible to independently determine the sound pressure of the incident wave (p_i) and that of the reflected wave (p_r). Subsequently, the sound pressure reflection coefficient (r) at the specimen surface is defined as the ratio of the reflected to the incident sound pressure, expressed as

$$r=\frac{p_r}{p_i}. \tag{22}$$

According to the principle of conservation of sound energy, the normal sound absorption coefficient α for the material under normal incidence can be expressed as

$\alpha = 1\text{-}|r|^2.$ (23)

Subsequently, the computational analysis system generates essential acoustic parameters, including the sound absorption coefficient and the characteristic acoustic impedance, thereby enabling a comprehensive quantitative assessment of the material's acoustic properties under normal incidence.

3.2.2. Sound insulation performance testing using the reverberation chamber method

Sound insulation, quantified by sound transmission loss, constitutes a fundamental metric for evaluating the acoustic performance of materials. The underlying physical mechanism encompasses the combined effects of sound wave reflection at material interfaces and the internal dissipation of acoustic energy, resulting in the effective attenuation of sound transmission. To tackle the complexities associated with random incident noise impacting electric vehicle doors, this research utilizes a hybrid finite element-statistical energy analysis (FE-SEA) approach to develop a coupled simulation model integrating a reverberation chamber and composite panels within the VA One software environment. This methodology facilitates the accurate characterization and quantification of the sound insulation properties of the materials under investigation.

The simulation model is founded on the principle of power flow equilibrium within the framework of statistical energy analysis. Both the sound-emitting and receiving chambers are represented as environments characterized by uniformly diffuse sound fields. Sound waves impinge upon the surface of the composite panel in a stochastic manner, with a fraction of the acoustic energy transmitted through the panel into the receiving chamber. The sound insulation performance is quantified by calculating the difference in sound field energy between the two chambers, subsequently adjusted to account for the equivalent sound absorption properties of the receiving chamber. An acoustic cavity consisting of dual reverberation chambers was developed utilizing the Great Cube plugin integrated within the software. The composite panel was represented through a multi-layer configuration that accurately reflects the actual structural composition of the door acoustic package, with material properties assigned according to the nominal specifications of commercially available materials. The composite panel was modeled as a deterministic system employing a coupled Finite Element-Statistical Energy Analysis (FE-SEA) subsystem, whereas the sound field within the reverberation chambers was treated as a stochastic subsystem using the Statistical Energy Analysis (SEA) approach. Coupling of energy transfer between these subsystems was facilitated via surface connections, thereby enabling comprehensive characterization of sound insulation performance across the full frequency spectrum. To replicate the real-world external noise environment, a 1 Pa random plane wave excitation was applied to the sound source chamber. The overall configuration of the model is illustrated in Fig. 6.

The determination of the core sound insulation index is derived from the disparity in sound pressure levels measured between the two spaces, adjusted to account for the equivalent sound absorption characteristics of the receiving room. The resulting formula is as follows:

$$STL = SPL_1 - SPL_2 + 10\lg\frac{S}{A}. \tag{24}$$

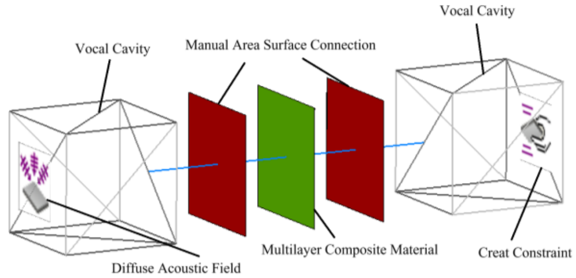

Fig. 6. Schematic diagram of reverberation chamber method model establishment

In the presented equation, SPL_1 and SPL_2 denote the sound pressure levels averaged over 1/3-octave bands (measured in decibels) within the sound-emitting chamber and the receiving chamber, respectively. The variable S corresponds to the effective test area of the composite panel, expressed in square meters (m²). Additionally, A represents the equivalent sound absorption area of the receiving chamber (m²), which is determined automatically by the simulation model through an iterative procedure grounded in the assumption of a diffuse sound field.

4. ACOUSTIC PERFORMANCE ANALYSIS BASED ON THE TRANSFER MATRIX METHOD

4.1. The influence of porosity on acoustic properties

To investigate the effect of glass fiber porosity on the acoustic characteristics of the composite, the porosity φ was set to 0.94, 0.7, and 0.5, while all other structural parameters were kept constant. The sound absorption coefficient, acoustic impedance coefficient, and reflection coefficient were calculated using the transfer matrix method. The results are presented in Fig. 7 – Fig. 9.

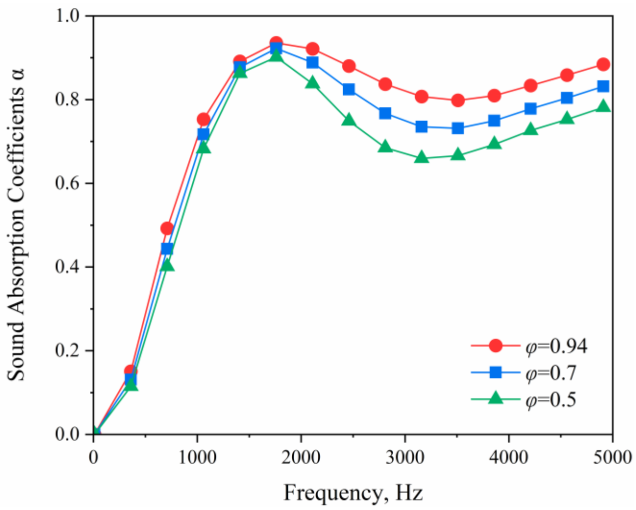

Fig. 7. Influence of the porosity of light wool on the absorption coefficient

Fig. 7 shows that in the low-frequency range (10 – 1000 Hz), the absorption coefficients for all three porosity levels are low and exhibit negligible differences, indicating that porosity has little influence in this band.

In the mid-frequency range (1000 – 3000 Hz), the absorption coefficient increases markedly, with peaks exceeding 0.9; higher porosity yields marginally better absorption. In the high-frequency range (3000 – 5000 Hz), the absorption coefficient generally declines, but high-porosity materials maintain relatively better performance, while low-porosity materials show the strongest decrease. Hence, increasing porosity expands the effective sound absorption bandwidth in the mid-to-high frequencies and preserves absorption efficiency at high frequencies.

Fig. 8 presents the acoustic impedance coefficient. In the low-frequency range (10 – 2000 Hz), the impedance curves for different porosity levels nearly coincide, consistent with the weak sensitivity of low-frequency absorption to porosity.

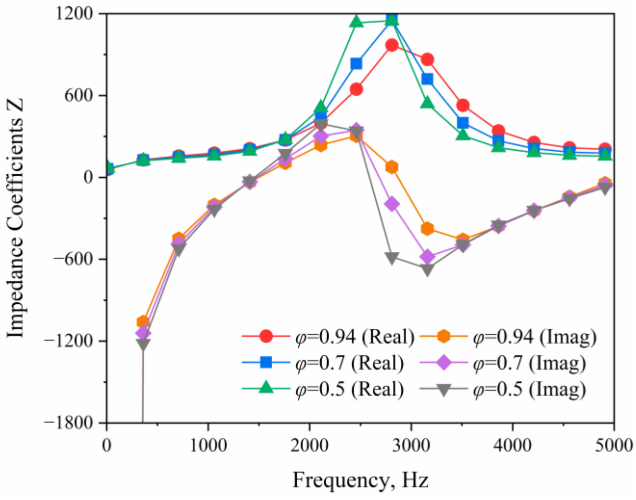

Fig. 8. Influence of the porosity of light glass wool on the impedance

In the low-to-mid transition region (2000 – 2900 Hz), low-porosity materials exhibit higher acoustic resistance (real part). In the mid-to-high frequency range (2900 – 4000 Hz), high-porosity materials reach a peak in resistance. Notably, in the 2500 – 3500 Hz band, high-porosity materials simultaneously show moderate real impedance and a small absolute value of imaginary impedance (reactance), which improves impedance matching with air and promotes sound wave penetration rather than reflection.

Fig. 9 illustrates the reflection coefficient. In the low-frequency range (10 – 1500 Hz), the real part declines rapidly and curves overlap, confirming the minor role of porosity. In the mid-frequency range (1500 – 3000 Hz), low-porosity ($\varphi = 0.5$) materials exhibit a higher real part of the reflection coefficient; their imaginary part absolute value is consistently larger than that of high-porosity materials from 2000 Hz upward. This indicates stronger reflection and more pronounced impedance effects for low-porosity materials in the mid-frequency range. In the high-frequency range (3000 – 5000 Hz), the real part decreases again, and high-porosity materials show a slightly higher reflection coefficient, though the difference narrows.

In summary, increasing porosity improves impedance matching in the mid-frequency range (1500 – 3500 Hz), thereby reducing sound reflection and raising the absorption coefficient above 0.9, while also broadening the effective absorption bandwidth.

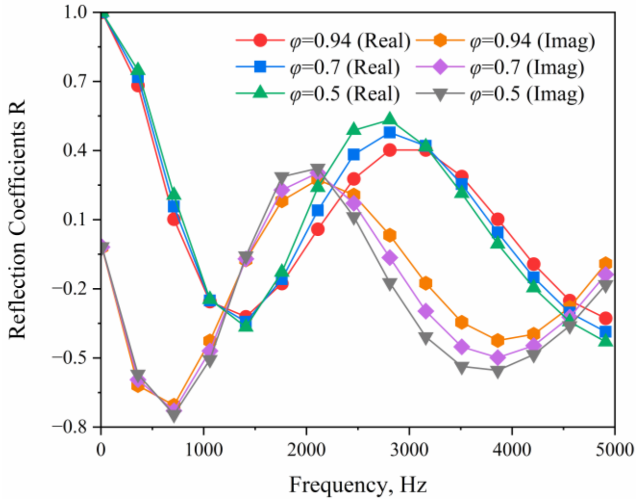

Fig. 9. Influence of the porosity of light glass on the reflection coefficient

High porosity also maintains relatively good absorption in the high-frequency range (3000 – 5000 Hz). In contrast to the gradient porous design introduced by Fei Wu et al. [22], the present study elucidates the physical mechanism through which porosity governs impedance matching and reflection suppression in a single-layer composite structure. This approach avoids the complexities of multi-layer interfaces and multi-parameter coupled optimization, achieving efficient broadband mid-to-high frequency absorption with a simpler configuration. Consequently, these findings provide practical and streamlined design principles for engineering noise reduction applications.

4.2. The influence of air backing layer thickness on acoustic properties

To examine the mechanism by which the thickness of the air backing layer affects acoustic performance, the thickness d was varied as 20 mm, 10 mm, and 5 mm, while other parameters remained unchanged. The absorption, impedance, and reflection coefficients were computed using the transfer matrix method (Fig. 10 – Fig. 12).

Fig. 10 demonstrates that in the low-to-mid frequency range (10 – 2500 Hz), the absorption coefficient increases with frequency for all thicknesses, and the rate of increase is positively correlated with the backing layer thickness. The thickest backing (d = 20 mm) gives the best low-to-mid frequency absorption, suggesting that a thicker air layer significantly enhances low-frequency absorption. In the mid-to-high frequency range (2500 – 5000 Hz), absorption coefficients for all three configurations stabilize above 0.8, with the thinnest backing (d = 5 mm) performing marginally better. Thus, increasing the backing thickness optimizes low-frequency absorption, while reducing thickness preserves high efficiency at mid-to-high frequencies.

Fig. 11 shows the impedance coefficient. In the low-frequency range (10 – 1500 Hz), the real part is insensitive to thickness, and the curves largely overlap.

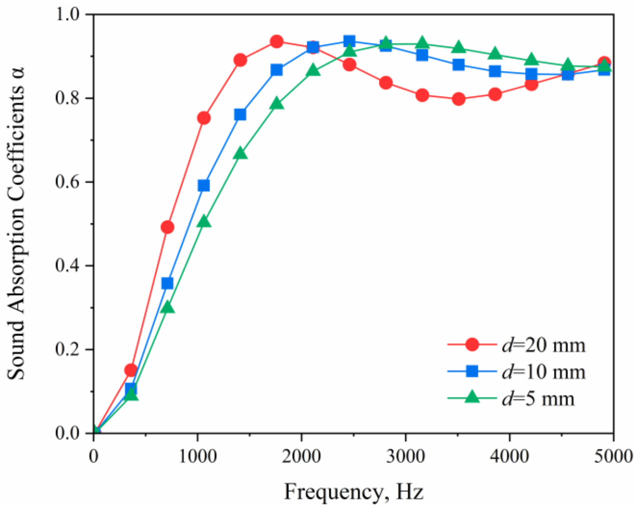

Fig. 10. Influence of the air layer thickness of glass fiber mat on the absorption coefficient

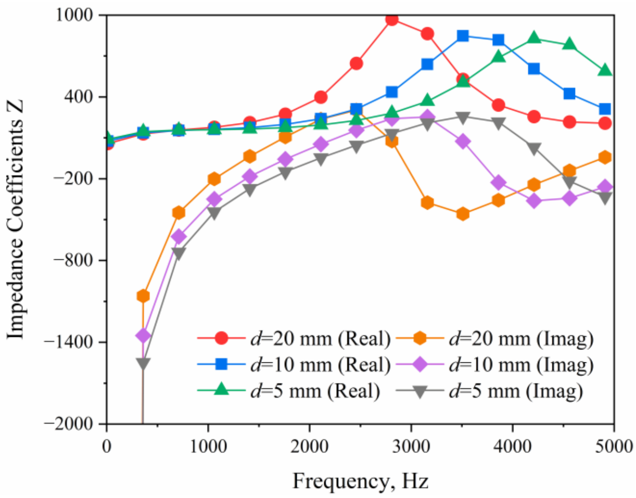

Fig. 11. Influence of the air layer thickness of glass fiber mat on the impedance

In the mid-frequency range (1500 – 3000 Hz), the real part for $d = 20$ mm rises rapidly, peaking at 2900 Hz; for $d = 10$ mm and 5 mm, the peaks shift to 3500 Hz and 4000 Hz, respectively. For the imaginary part, its absolute value is smaller for $d = 20$ mm in the low-to-mid frequency range (10 – 2900 Hz), but becomes significantly larger in the mid-to-high range (2900 – 4000 Hz). This confirms that increasing the backing layer thickness shifts the impedance peak and reflection characteristics toward lower frequencies, improving impedance matching and reducing reflections in the low-to-mid range, but at the cost of increased imaginary impedance magnitude and stronger reflections in the mid-to-high range.

Fig. 12 displays the reflection coefficient. In the low-frequency range (10 – 1500 Hz), the real part generally decreases, and a thinner backing layer gives a larger real part. In the mid-frequency range (1500 – 3500 Hz), the real part for $d = 20$ mm first increases and then decreases, reaching a maximum at 3000 Hz; the peaks for $d = 10$ mm and 5 mm shift to 3800 Hz and 4400 Hz, respectively. For the imaginary part, the absolute value for $d = 20$ mm is smaller in the 800 – 2500 Hz range (weaker reflection) but larger in the 2500 – 4500 Hz range (stronger reflection). Therefore, a thicker backing layer reduces reflection in the low-to-mid range but increases reflection in the mid-to-high range.

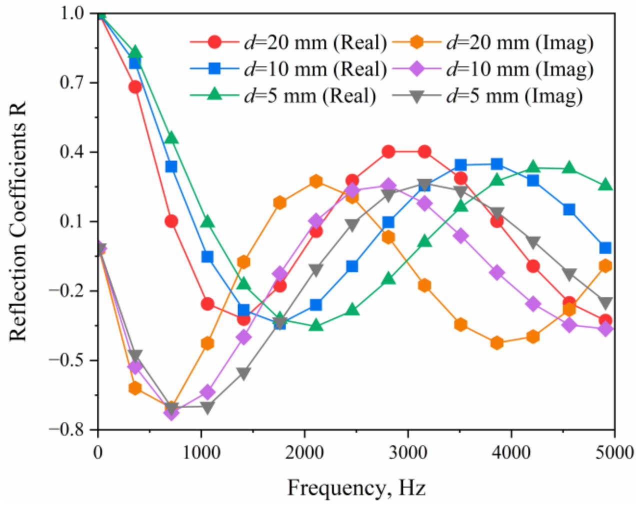

Fig. 12. Influence of the air layer thickness of glass fiber mat on the reflection coefficient

In summary, increasing the backing layer thickness shifts the impedance peak and reflection characteristics to lower frequencies, thereby improving low-to-mid frequency absorption but reducing mid-to-high frequency absorption. Conversely, a thinner backing layer is better for maintaining high absorption efficiency at mid-to-high frequencies. Consequently, the choice of backing thickness should be based on the target noise spectrum: a thicker layer for low-frequency noise, a thinner layer for mid-to-high frequency noise.

4.3. The influence of flow resistance on acoustic properties

To investigate how flow resistivity affects the acoustic properties, σ was set to 10000, 20000, and 30000 Pa·s/m^2, with all other parameters held constant. The absorption, impedance, and reflection coefficients were calculated using the transfer matrix method (Fig. 13 – Fig. 15).

Fig. 13 indicates that in the low-frequency range (10 – 1800 Hz), the absorption coefficient increases rapidly with frequency, and higher flow resistivity yields a higher absorption coefficient. This means that high flow resistivity enhances viscous dissipation within the pores, thereby improving absorption capacity. Above 1800 Hz, the absorption curves decline slightly but remain above 0.75, and high σ materials maintain a marginal advantage. Hence, high flow resistivity benefits broadband absorption across the entire frequency range.

Fig. 14 shows that the real part of the impedance coefficient exhibits notable peak variations mainly in the mid-frequency range (2500 – 3500 Hz), where low σ gives the highest real peak. The imaginary part behaves differently in two intervals: its absolute magnitude is smaller in the low-to-mid range (1800 – 3000 Hz) and larger in the mid-to-high range (3000 – 4500 Hz). In other frequency bands, the impedance curves converge. Thus, flow resistivity primarily affects impedance matching by modulating the real impedance peak in the mid-frequency range and the imaginary part characteristics in the transition region between low and high frequencies.

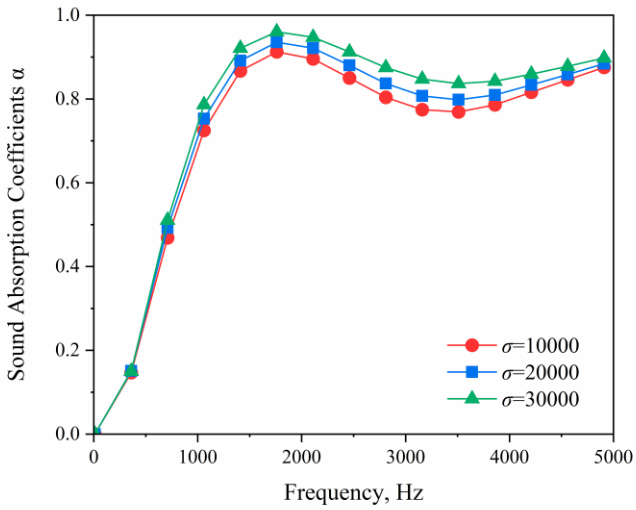

Fig. 13. Influence of the resistance of glass fiber mat on the absorption coefficient

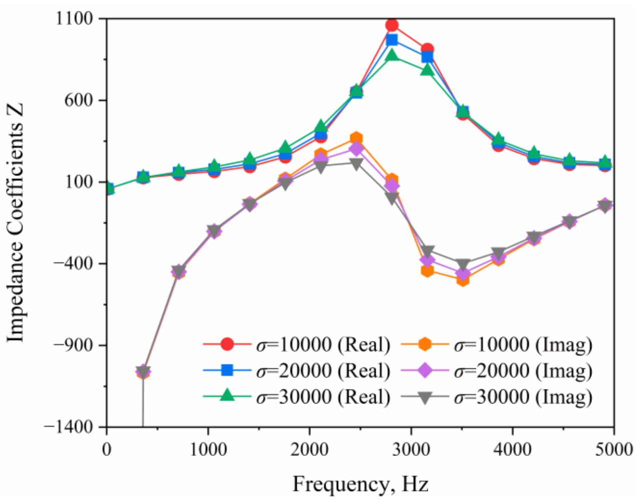

Fig. 14. Influence of the resistance of glass fiber mat on the impedance

Fig. 15 presents the reflection coefficient. In the low-to-mid frequency range (1000 – 2200 Hz), high σ materials exhibit a larger real part of the reflection coefficient; in the mid-to-high range (2200 – 4000 Hz), their real part becomes smaller. Additionally, in the 1500 – 4500 Hz interval, low σ materials show a larger absolute imaginary part of the reflection coefficient. Therefore, flow resistivity influences the acoustic response mainly by altering the reflection properties in the transition region between low-to-mid and mid-to-high frequencies.

In summary, high flow resistivity (σ = 30000) improves low-to-mid frequency absorption through enhanced viscous dissipation and maintains absorption advantages over the full spectrum, but it reduces the real impedance peak and increases the real part of the reflection coefficient in the low-to-mid range. Low flow resistivity (σ = 10000) gives slightly lower low-to-mid absorption but offers a higher real impedance peak at mid frequencies and a larger imaginary reflection amplitude, which benefits impedance matching and phase control.

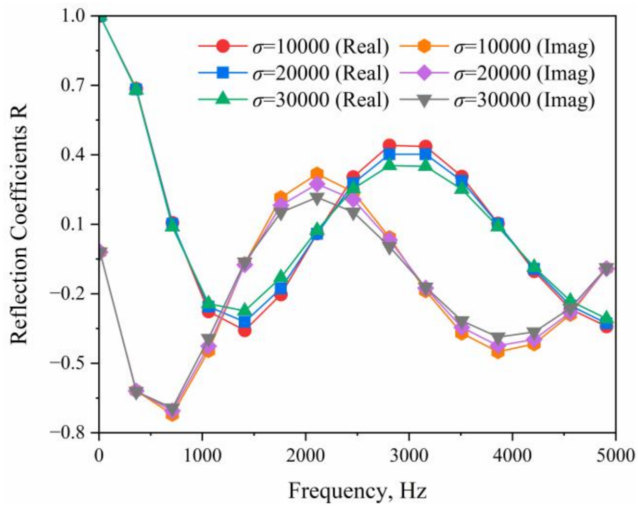

Fig. 15. Influence of the resistance of glass fiber mat on the reflection coefficient

Therefore, the choice of flow resistivity should be tailored to the target noise band: high σ is preferable for low-to-mid frequency noise, while low σ is better for mid-frequency impedance matching and phase management.

5. SOUND INSULATION PERFORMANCE AND STRUCTURAL OPTIMIZATION BASED ON THE FE-SEA HYBRID METHOD

5.1. Comparison of sound insulation performance among different layering schemes

To elucidate the acoustic control mechanisms of composite structures within the confined space of a car door (total thickness ≤ 45 mm, 19 mm gap between inner and outer panels), sound transmission loss (STL) calculations under random incident excitation were performed for the five layup schemes listed in Table 2 using a hybrid FE-SEA model. In all schemes, the steel plate thickness was fixed at 1 mm, and the GF-MF composite thickness was maintained at 25 mm; the only variable was the intermediate layer. The analysis below is conducted separately based on the positions of the honeycomb material and the damping layer.

Fig. 16 presents the results pertaining to the sound insulation performance of three door composite structure layup schemes (Schemes 1, 2, and 3). The data reveal a characteristic increase in sound insulation with rising frequency. Notably, the core variables-specifically the honeycomb and backing structures-exert a frequency-dependent influence on sound insulation efficacy. In the low-frequency domain (10 – 1000 Hz), Scheme 1 demonstrates the most rapid improvement in sound insulation. This superior performance is attributed to the elastic cushioning effect of the air backing layer, which effectively suppresses low-frequency structural sound transmission. Conversely, the high stiffness inherent to the honeycomb panel in other schemes tends to induce structural resonance within this frequency range, thereby diminishing sound insulation capabilities.

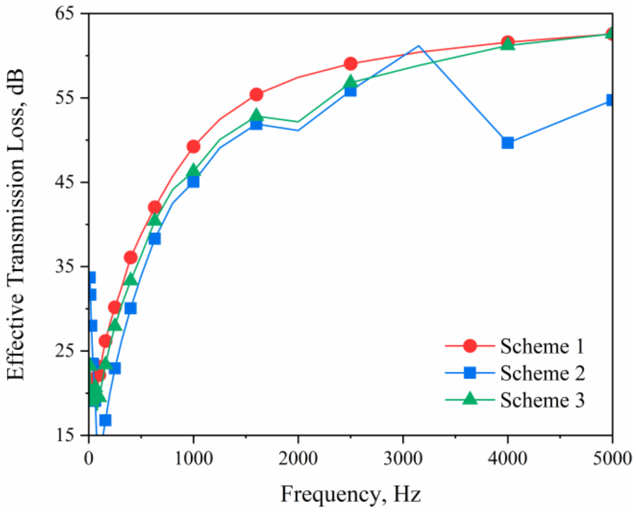

Fig. 16. Sound transmission loss of schemes 1, 2 and 3

Within the mid-frequency range (1000 – 3000 Hz), all three schemes exhibit continued enhancement in sound insulation. Scheme 1 consistently outperforms the others, Scheme 3 shows a gradual convergence towards Scheme 1's performance, while Scheme 2 remains comparatively less effective. This trend suggests that the interplay between structural stiffness and the porous sound-absorbing layer becomes the predominant factor influencing sound insulation in this frequency band. In the mid-to-high frequency range (3000 – 5000 Hz), Schemes 1 and 3 maintain stable and elevated sound insulation levels exceeding 60 dB, with their performances converging. In contrast, Scheme 2 experiences a pronounced decline followed by a gradual recovery. These observations imply that the sound insulation in Schemes 1 and 3 within this frequency range is primarily governed by the porous sound-absorbing properties of non-reinforced glass fiber and melamine foam. Meanwhile, the aluminum honeycomb panel's structural characteristics contribute to fluctuations in sound insulation performance in the mid-to-high frequency spectrum. Overall, Scheme 1 demonstrates the most comprehensive sound insulation performance across the entire frequency range, with a particularly marked advantage in the low-frequency region. This finding is consistent with the observations of Su et al. [9], who reported that an air backing layer improves low-frequency STL more effectively than a honeycomb core in firewall structures. However, unlike [9], the present study further quantifies the degradation caused by the honeycomb layer (Schemes 2 and 3) under the same total thickness constraint. Consequently, Scheme 1 emerges as the optimal structural configuration among the three for vehicle door noise mitigation.

Fig. 17 presents the results regarding the effective sound insulation of the composite door structure in Scheme 4. The sound insulation performance demonstrates pronounced frequency-dependent behavior and is influenced by the positioning of the damping layer. Within the low-frequency range (10 – 2000 Hz), Scheme 4 consistently achieves the highest sound insulation, followed by Scheme 1, which lacks a damping layer, while Scheme 5 exhibits substantially lower sound insulation compared to the other two schemes. This disparity arises because situating the damping layer adjacent to the steel panel directly attenuates the panel's structural vibrations, thereby effectively obstructing low-frequency structural sound transmission paths. Conversely, positioning the damping layer behind the panel considerably diminishes its capacity to suppress panel vibrations. In the high-frequency range (2000 – 5000 Hz), the sound insulation performance of Scheme 5 increases markedly, surpassing that of both Scheme 4 and Scheme 1.

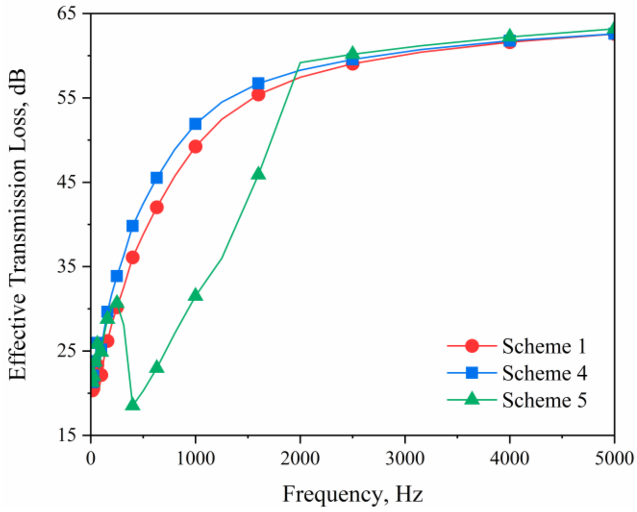

Fig. 17. Sound transmission loss of Schemes 1, 4 and 5

Additionally, the sound insulation levels of all three schemes tend to converge as frequency increases, suggesting a reduced influence of structural damping in this range and a predominance of sound energy dissipation by the porous acoustic layer. The configuration with the damping layer mounted at the rear is more favorable for sound energy dissipation in the mid-to-high-frequency spectrum. Overall, Scheme 4 demonstrates superior sound insulation performance in the low-frequency domain, thereby better satisfying practical requirements for mitigating road noise, wind noise, and other relevant noise frequencies in automotive doors. Consequently, Scheme 4 is identified as the optimal structure for low-frequency noise control in car door applications.

5.2. Co-optimization of parameters for the optimal layering scheme

As shown in Fig. 18, based on the preferred design (Scheme 1) identified in Section 5.1, the optimal material parameters obtained in Chapter 4 were incorporated: the porosity of the unreinforced glass fiber was set to 0.94, and the flow resistance was set to 30,000 Pa·s/m² (high flow resistance is beneficial for sound absorption in the low-to-mid frequency range). At the same time, the damping layer configuration from Scheme 4 was retained (2 mm butyl rubber in direct contact with the steel plate side). FE-SEA simulation results indicate that, after applying the optimized parameters, the STL of the composite structure in the 100-1000 Hz low-frequency range improved by an average of approximately 1.5 – 2.5 dB compared to the initial parameters, validating the effectiveness of the synergistic optimization of material parameters and structural layering.

5.3. Analysis of modal evolution characteristics in the mid-to-high frequency range

To assess the suitability of the FE-SEA hybrid method within the mid-to-high frequency domain, the panel subsystem from Scheme 1 was chosen as the focal point of analysis. The investigation was carried out by examining both the modal behavior and the statistical properties of the system.

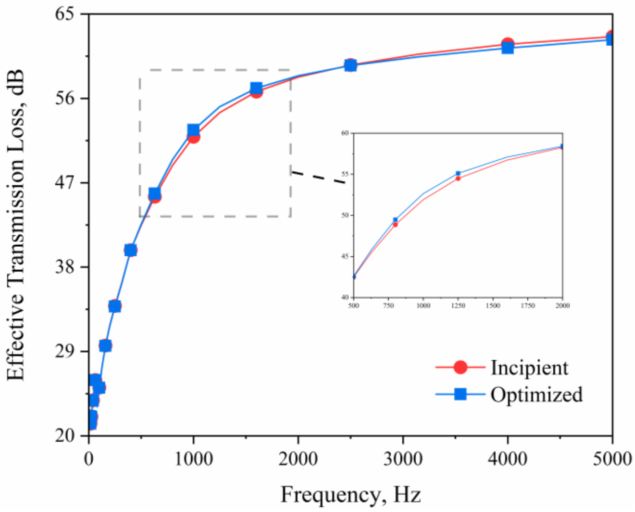

Fig. 18. Joint optimization of parameters and transmission loss

Initially, modal displacement contour plots were obtained at three representative frequencies 1500 Hz, 2500 Hz, and 3500 Hz as illustrated in Fig. 19 – Fig. 21. The modal patterns demonstrate a clear evolutionary progression with increasing frequency.

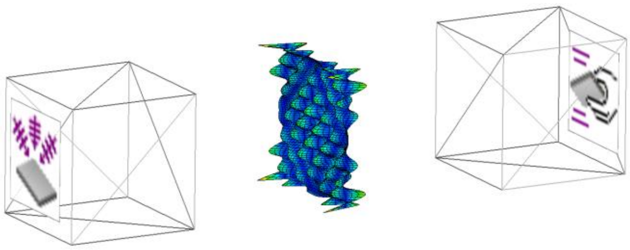

Fig. 19. Mode displacement contour plot at 1500 Hz

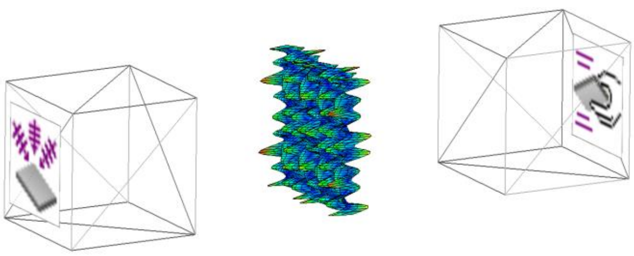

Fig. 20. Mode displacement contour plot at 2500 Hz

At 1500 Hz, the modal distribution is relatively sparse, with vibrations predominantly localized along the plate edges or confined to small central areas, characteristic of low-frequency localized vibration modes. As the frequency increases to 2500 Hz, the modal shapes become more intricate, the regions of vibration expand, and multiple peaks emerge in an alternating pattern, suggesting a transition of the structure from deterministic vibration behavior toward statistical uniformity. At 3500 Hz, the modal density rises substantially, the displacement distribution becomes highly irregular and encompasses the entire domain, and there is a pronounced increase in modal overlap.

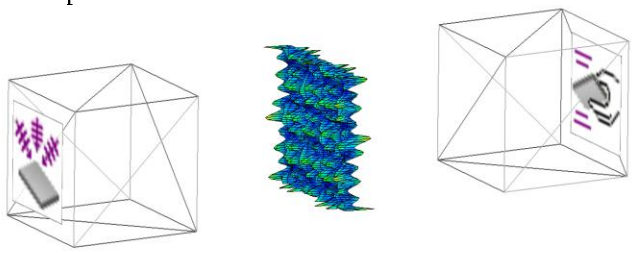

Fig. 21. Mode displacement contour plot at 3500 Hz

The “Modes in Band” for this subsystem were extracted within the 1/3-octave frequency bands from the model, with the results presented in Fig. 22. It is evident that the number of modes increases markedly as frequency rises, reaching 18.3 modes in the 1000 Hz band and 45.9 modes in the 2500 Hz band.

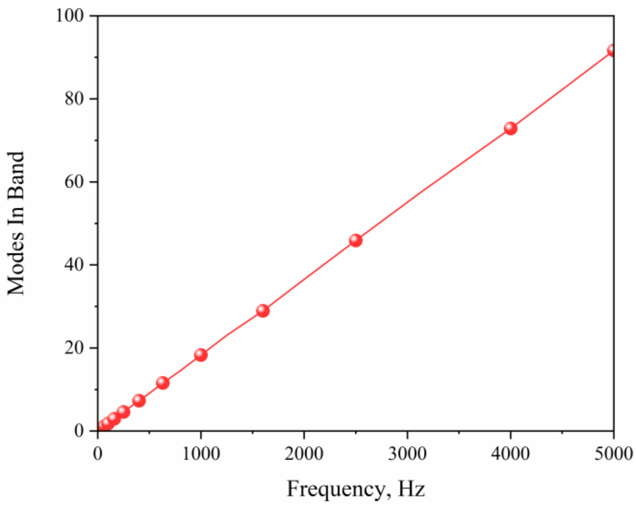

Fig. 22. Number of modes per 1/3 octave frequency band

According to the fundamental criteria of statistical energy analysis (SEA), the mode overlap assumption is considered valid when the number of modes per analysis band exceeds five, resulting in system responses that exhibit statistically averaged behavior. In this investigation, all frequency bands above 1000 Hz meet this criterion. Nevertheless, the modal cloud plot reveals that only at frequencies exceeding 2500 Hz do the modal shapes become sufficiently complex and demonstrate global participation, thereby fulfilling the stringent SEA requirements concerning system randomness. The high modal density above 2500 Hz confirms that the SEA assumptions are fulfilled, thereby establishing the methodological applicability of the hybrid FE-SEA approach for this composite structure in the mid-to-high frequency range. It should be noted that the modal analysis serves not as a validation of absolute numerical accuracy, but to ensure the validity of comparative assessments. Under identical modeling conditions, the relative STL differences between different layup schemes (e.g., Scheme 4 outperforming Scheme 1 by approximately 3 dB in the low-frequency range) are considered reliable for engineering comparison. Based on the parameter sensitivity analysis in Section 4 (flow resistivity ± 20 %, porosity ± 5 %), the expected numerical uncertainty of the predicted STL is approximately ± 2 dB in the low-to-mid frequency range. This estimate accounts for typical batch variations of the material properties. Because all layup schemes are compared under identical model settings, the relative STL differences between schemes are considered reliable.

6. CONCLUSIONS

1. Low-frequency (≤ 1000 Hz) absorption of GF-MF composites is governed mainly by air backing thickness and structural resonance. In the mid-frequency range (1000 – 3000 Hz), higher GF porosity increases the absorption coefficient, and higher flow resistivity enhances mid-to-low frequency attenuation via viscous friction. Above 3000 Hz, absorption is dominated by the material's inherent viscous-thermal properties, with structural parameters playing a minor role.
2. Under the 45 mm thickness limit, placing a 2 mm viscoelastic damping layer directly on the outer door panel (Scheme 4) improves low-frequency STL by approximately 3 dB compared to the pure air layer (Scheme 1). Positioning the damping layer on the GF-MF side (Scheme 5) reduces low-frequency STL relative to the undamped case due to greater distance from the vibration source. Honeycomb sandwich structures (Schemes 2 and 3) create additional solid-to-solid transmission paths, resulting in lower STL than the pure air layer.
3. To effectively mitigate structural noise, the damping layer must remain in intimate contact with the steel panel. Scheme 4 (damping layer on the steel side) is therefore the optimal configuration for low-frequency noise control. The recommended scheme combines a pure air layer with a steel-side damping layer and optimized material parameters (GF porosity 0.94, flow resistivity 30000 Pa·s/m²), achieving enhanced STL across the full frequency spectrum and notably improved suppression of low-frequency road noise.

Acknowledgments

Supported by Natural Science Foundation of Heilongjiang Province (LH2024E021).

REFERENCES

1. **Andrea, S., Paolo, B., Aurora, M., Cristina, M., Francesco, P., Patrizio, F.** A Hybrid Approach for Modelling the Acoustic Properties of Recycled Fibre Mixtures for Automotive Applications *Applied Acoustics* 182 (c) 2021: pp. 108272. https://doi.org/10.1016/j.apacoust.2021.108272
2. **Jiang, Y., Bai, G., Sui, F., Shen, X.** Study on Acoustic Properties of Multilayer Composite Materials *Environmental Engineering* 30 (S1) 2012: pp. 211 – 213. https://doi.org/10.13205/j.hjgc.2012.s1.059
3. **Kim, J., Choi, E., Jeon, W.** Lightweight Soundproofing Meta-Panel for Separate Wide Frequency Bands *Mechanical Systems and Signal Processing* 184 (c) 2023: pp. 109647. https://doi.org/10.1016/j.ymssp.2022.109647
4. **Sangiuliano, L., Reff, B., Palandri, J., Wolf-Monheim, F., Pluymers, B., Deckers, E., Desmet, W., Claeys, C.** Low Frequency Tyre Noise Mitigation in a Vehicle Using Metal 3D Printed Resonant Metamaterials *Mechanical Systems and Signal Processing* 2022: pp. 179. https://doi.org/10.1016/j.ymssp.2022.109335
5. **Jung, J., Kim, H., Goo, S., Chang, K., Wang, S.** Realisation of a Locally Resonant Metamaterial on the Automobile Panel Structure to Reduce Noise Radiation *Mechanical Systems and Signal Processing* 122 (c) 2019: pp. 206 – 231. https://doi.org/10.1016/j.ymssp.2018.11.050
6. **Kronowetter, F., Wagner, P., Kolodi, J., Brabandt, I., Neumeyer, T., R ü mmler, N., Marburg, S.** Novel Compound Material and Metamaterial Wheelhouse Liners for Tire Noise Reduction *Mechanical Systems and Signal Processing* 200 (c) 2023: pp. 110548. https://doi.org/10.1016/j.ymssp.2023.110548
7. **O'Boy, M., Daniel, J.** Automotive Wheel and Tyre Design for Suppression of Acoustic Cavity Noise Through the Incorporation of Passive Resonators *Journal of Sound and Vibration* 47 (4) 2020: pp. 467. https://doi.org/10.1016/j.jsv.2019.115037
8. **Hwang, H.D., Maxit, L., Ege, K., Gerges, Y., Guyader, J.L.** SmEdA Vibro-acoustic Modelling in the Mid-frequency Range Including the Effect of Dissipative Treatments *Journal of Sound and Vibration* 393 2017: pp. 187 – 215. https://doi.org/10.1016/j.jsv.2017.01.024
9. **Su, J., Zheng, L.** Study on the Acoustic Performance Mechanism of a New Type of Composite Structure in Vertical Incidence and Diffusion Domain *Journal of Mechanical Engineering* 57 (17) 2021: pp. 149 – 162. https://doi.org/10.3901/JME.2021.17.149
10. **Zhou, G., Wu, J., Lu, K., Tian, X.** Broadband Low-Frequency Membrane-Type Acoustic Metamaterials with Multi-State Anti-Resonances *Applied Acoustics* 159 2020: pp. 107078. https://doi.org/10.1016/j.apacoust.2019.107078
11. **Wang, X., Ma, L., Wang, Y., Guo, H.** Design of Multilayer Sound-Absorbing Composites with Excellent Sound Absorption Properties at Medium and Low Frequency Via Constructing Variable Section Cavities *Journal of Mechanical Engineering* 266 2021: pp. 113798. https://doi.org/10.1016/j.compstruct.2021.113798
12. **Shen, L., Zhang, H., Lei, Y., Chen, Y.** Hierarchical Pore Structure Based on Cellulose Nanofiber/Melamine Composite Foam with Enhanced Sound Absorption Performance *Carbohydrate Polymers* 255 2021: pp. 117405. https://doi.org/10.1016/j.carbpol.2020.117405
13. **Shen, X., Bai, P., Chen, L., To, S., Yang, F., Zhang, X., Yin, Q.** Development of Thin Sound Absorber by Parameter Optimization of Multilayer Compressed Porous Metal with Rear Cavity *Applied Acoustics* 159 2020: pp. 107071. https://doi.org/10.1016/j.apacoust.2019.107071
14. **Wan, Q., Liu, X., Gu, B., Bai, W., Su, C., Deng, Y.** Thermal and Acoustic Performance of an Integrated Automotive Thermoelectric Generation System *Applied Thermal Engineering. Design, Processes, Equipment, Economics* 158 2019: pp. 8. https://doi.org/10.116/j.applthermaleng.2019.113802
15. **Shen, J., Fu, S., Su, R., Xu, H., Lu, Z., Zeng, F., Cheng, S., Wang, W., Feng, P.** A Multilayered Structure for Packageless Acoustic- Wave Devices with Ultra-Small Sizes

Journal of Microelectromechanical Systems 30 (4) 2021: pp. 589 – 596. https://doi.org/10.1109/JMEMS.2021.3074385

16. **Otaru, A.J.** Research of the Numerical Simulation and Machine Learning Backpropagation Networks Analysis of the Sound Absorption Properties of Cellular Soundproofing Materials *Results in Engineering* 31 (5) 2011: pp. 586 – 590. https://doi.org/10.1016/j.rineng.2023.101588
17. **Chen, L., Du, L., Wang, X., Sun, X.** An Extended Transfer Matrix Method for Measuring Acoustical Properties of Porous Materials Beyond the Cut-Off Frequency *The Journal of the Acoustical Society of America* 148 (6) 2020: pp. 3772 – 3783. https://doi.org/10.1121/10.0002940
18. **Huo, R., Chen, L., Liu, J., Peng, D.** The Application of Transfer Matrix Method in Acoustic Performance Analysis of Composite Materials and Acoustic Protection Design of Ship *Materials Science and Engineering* 544 2019: pp. 1 – 6. https://doi.org/10.1088/1757-899X/544/1/012047
19. **Chen, P., Shen, H., Zhang, J., Xiao, X.** The Effect of Temperature on the Acoustic Properties of Aluminum Profiles Coated with Damping Layer *Noise and Vibration Control* 37 (2) 2017: pp. 121 – 126. https://doi.org/10.3969/j.issn.1006-1355.2017.02.025
20. **Su, J., Li, X., Yang, H., Wu, T.** Research on Acoustic and Parametric Coupling of Single-Layer Porous Plate–Lightweight Glass Wool Composite Structure Doors for Pure Electric Vehicles *World Electric Vehicle Journal* 16 (7) 2025: pp. 393. https://doi.org/10.3390/wevj16070393
21. **Su, J., Liu, W., Huang, N.** Research on Optimization of Acoustic Packaging Performance of Electric Vehicle Motor Compartment Based on Transfer Matrix Theory *Materials Science* 2025: pp. 42507. https://doi.org/10.5755/j02.ms.42507
22. **Wu, F., Zhang, X., Ju, Z., Zhao, J., Hu, M., Gao, M., Luo, J. and Pu, H.** Ultra-Broadband Sound Absorbing Materials Based on Periodic Gradient Impedance Matching *Frontiers in Materials* 9 2022: pp. 909666. https://doi.org/10.3389/fmats.2022.909666